DOI: 10.37190/ABB-02463-2024-03

Assessment of Material Properties in Key Components of the Porcine Crystalline Lens During Overshooting

Milad Salimibani[1*], Ali Dahaghin[1], Agnieszka Boszczyk[1], Jorge Grasa[2], Damian Siedlecki[1]

[1]Department of Optics and Photonics, Wroclaw University of Science and Technology, Wrocław, Poland

[2]Aragón Institute of Engineering Research (I3A), University of Zaragoza, Zaragoza, Spain

[*]Corresponding author: Milad Salimibani, Department of Optics and Photonics, Wroclaw University of Science and Technology, Wrocław, Poland, e-mail address: milad.salimibani@pwr.edu.pl

Submitted: 6th June 2024

Accepted: 10th November 2024

Abstract

Purpose: The porcine eye serves as a valuable surrogate for studying human ocular anatomy and physiology because of its close resemblance. This study focuses on the influence of material properties, specifically Young's modulus and Poisson's ratio, on the crystalline lens overshooting amplitude during rapid eye rotation.

Methods: The Finite Element Method (FEM) is employed to explore various material property scenarios, and sensitivity analysis is conducted to assess their impact on the mechanical displacement of the crystalline lens apex. The measurements were made of three output parameters: maximum displacement, time of maximum displacement appearance , and stabilization time.

Results: The results highlight the significance of fine-tuning of the zonule's material properties, particularly Young's modulus, in achieving a reliable model. They suggest that fine-tuning of these parameters can lead to a highly reliable model, enabling in-depth research in the opto-dynamic simulations.

Conclusions: Having a complete examination of crystalline lens displacement in *ex vivo* porcine eye models and detailing crucial factors for accurate modeling will open the path for future studies especially in conditions affected by dynamic aspects of the crystalline lens or in *in vivo* research.

Keywords: Crystalline lens overshooting, Finite element method, Sensitivity analysis, Fluid-structure interaction (FSI)

1. Introduction

The eye is a complex optical and mechanical system. It is a marvel of biological engineering that enables us to see the world around us with such a remarkable clarity. Central to this system are two crucial elements: the cornea and the crystalline lens. They help the eye to see clearly by refracting the light and focusing it at the right spot on the retina. The cornea contributes around 60% of the focusing power and the remaining is provided by the crystalline lens, which additionally plays a very crucial role in accommodation through modifying its geometrical shape resulting in eye's refractive power adjustment to near or far vision conditions [16,30].

The literature survey reveals a significant interest among engineers in numerical modeling of the eye. Researchers in this field have recognized the value and potential of using computational techniques to gain a deeper understanding of the complex mechanisms and behaviors of this vital part of the human body [12,22,31]. One of the main motivations behind the interest in numerical modeling is the ability to simulate and predict the behavior of anterior eye structures under different conditions and stimuli. This approach provides valuable information on the biomechanical forces, stresses, and strains experienced by ocular tissues during normal functioning or in response to external factors. By accurately capturing these interactions, researchers can better understand and address the underlying mechanisms of various eye diseases and conditions. However, the investigation of crystalline lens wobbling is a developing area, and only a few studies show progress in evaluating of the performance of biomechanical simulations [3,17]. Their findings, particularly the maximum lens displacement and stabilization time, have yet to demonstrate substantial agreement with data conducted *in vivo* experiments [28].

Recently, Dahaghin et al. [5] conducted a groundbreaking study in which they, for the first time, measured and modeled the crystalline lens overshooting phenomenon under *ex vivo* conditions. Briefly, crystalline lens overshooting is a phenomenon when the lens finely shifts from its normal position immediately after stopping the rotational movement of the eye globe (see Supplementary Materials 1 and 2 that visualize the lens' inertial overshooting motion and its representation as a supersposition of tilt and lateral displacement). Crystalline lens overshooting is a direct and measurable effect of intraocular inertia. This forementioned research sheds new light on the behavior of the crystalline lens, valuable insight into its dynamics inside the eye, as well as new challenges, such as the fact that the biomechanics of the eye may be significantly influenced by a wide range of parameters which the modeling approach should attempt to narrow. One of the key challenges of the study is the observed non-uniformity of captured or estimated data, i.e. due to intersubject variability. Each eye has its unique characteristics, such as variations in material properties and size, as well as physiological and environmental conditions. All of these factors may significantly influence the results of computational simulations [1,2,4,10]. In particular, material properties play a crucial role in the study and therefore still need to be addressed. They must be accurately analyzed using the most appropriate data. Therefore, realistic and reliable models that can take into account the effects of material properties can be used for future research and investigations.

Porcine eye may serve as an important tool for research, as it shares many similarities with human ocular anatomy and physiology. Scientists and ophthalmologists have increasingly recognized the importance of using *ex vivo* models to study eye diseases [11]. These models provide a reliable alternative to *in vivo* studies while retaining a high degree of similarity. Using computational methods, researchers can simulate, analyze and likely predict the complex structural behavior of the porcine eye, such as providing valuable information on its mechanical properties and response to external forces [32]. Accomplishment of these objectives, obtaining accurate material properties for ocular tissues are particularly essential for reliable finite element modeling (FEM). Characterization of material properties and model validation against experimental data are some of the challenges in FEM modeling of the porcine eye. The main goal of this study is to investigate and analyze the magnitude of the crystalline lens overshooting response to variations in material properties of some of the ocular structures, namely: sclera, cornea, ciliary muscle, crystalline lens and zonular fibers. Given the diverse mechanical properties documented in literature for eye components, the study acknowledges the significant impact that each of them can have on the outcomes. Finally, it yields a valid *in silico* model for *ex vivo* optomechanical simulations for future studies.

2. Materials and methods

Numerical model

In order to assess the influence of material properties on the crystalline lens overshooting amplitude, a 2D numerical model was implemented. This model used a generic porcine eye globe with several mechanical material properties subjected to a constant intraocular pressure (IOP), which were previously developed and calibrated using Purkinje images performance [5]. The preparation and final adjustments of the results and simulations were conducted using COMSOL Multiphysics (Version 5.6), taking into account the dynamic interaction between the solid structure of the eye tissues and the intraocular fluids, specifically the aqueous humor and vitreous body, where the behavior of one affects the other, such as the lens, which is surrounded by fluids. Figure 1a presents the geometry employed in this study using physiological and anatomical data recorded in research studies [18,23,25].

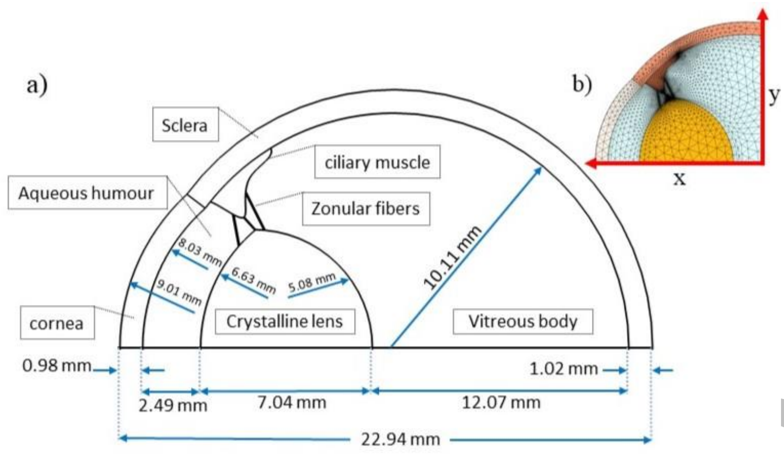

Figure 1. a) Dimensions of the finite element (FE) model. It includes the zonules, the lens, the ciliary muscle, the sclera, and cornea. b) Portion of the finite element mesh with the reference system located at the rotation center.

The crystalline lens is believed to hang on an eye globe with the support of three sets of zonular fibers: anterior, equatorial, and posterior, each having a thickness of 50 µm. Due to the lack of available data in the literature, the thickness used was taken from a human subject [15]. It is worth mentioning that several animals, such as porcines, rabbits, and cows, share some similarities in their eye structures with humans, but with some anatomical differences. For example, crystalline lens thickness in porcine is almost double [23].

Next the model was intended to reconstruct our *ex vivo* experimental conditions, which were presented previously [5]. For this purpose Figure 2, the eyeball model was subjected to 90 deg rotation around its vertical axis (which is perpendicular to the plane of the 2-D model) and the movement data for the apical point of the crystalline lens were captured.

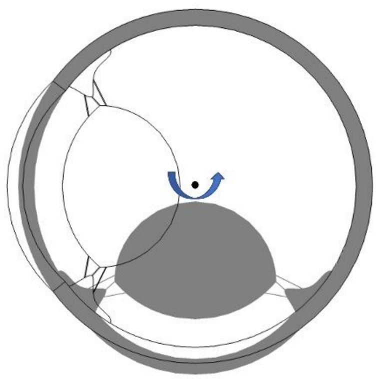

Figure 2. Direction of rotation of the eyeball by 90 degrees, starting from the initial state (white) and ending in the final state (gray). The pivot point of rotation is marked with a black dot and the arrow denotes the direction of rotation.

The maximum angular velocity of the eye during smooth rotation reached 1700 deg/s, which was set – again – in compliance with the *ex vivo* experiment conditions (this value was selected so that the angular acceleration of the eye *ex vivo* meets the order of magnitude of the angular acceleration of the human eye). Furthermore, the pivot point for rotation, located in the center of the eye globe, remained stationary without any linear movement. The governing equations and the boundary conditions were set the same as in our previous study [5]. The fluid dynamics around the eye were described by the time-dependent Navier-Stokes equations:

$$\rho \frac{\partial \mathrm{v}}{\partial \mathrm{t}} + \rho \nabla \cdot (\mathbf{v} \otimes \mathbf{v}) - \mu \nabla^2 \mathbf{v} + \nabla \mathrm{p} = \rho \mathbf{f}, \nabla \mathbf{v} = 0 \quad (1)$$

where **v** is the fluid velocity, p is the pressure, **f** represents volumetric forces, ρ is the density, and μ is the dynamic viscosity.

The mechanical behavior of the eye during rotation was modeled using multibody dynamics, assuming the sclera rotates without deformation. This was described by the following equation:

$$\rho \frac{\partial^2 \mathrm{u}}{\partial \mathrm{t}^2} = \nabla \cdot (\mathbf{FS})^{\mathrm{T}} + \rho \mathbf{f}, \mathbf{F} = \mathbf{I} + \nabla \mathbf{u} \quad (2)$$

where u is the displacement field, **F** is the deformation gradient tensor, **S** is the second Piola-Kirchhoff stress tensor, and **I** is the identity matrix.

The interactions between the fluid and solid components were captured using a fully coupled FSI approach, ensuring synchronized updates of the fluid and solid parameters:

$$\mathbf{f}_{\mathrm{a}} = [-\mathrm{p}\mathbf{I} + (\mu (\nabla \mathbf{v} + (\nabla \mathbf{v})^{\mathrm{T}}) - 2/3\, \mu (\nabla \cdot \mathbf{v}) \mathbf{I})] \cdot \mathbf{n}, \mathbf{v} = \frac{\partial \mathbf{u}_{\mathrm{soli}}}{\partial \mathrm{t}} \quad (3)$$

Mesh

In the described model, triangular elements were used to discretize both the solid and fluid domains. There were a total of 48,139 elements in this model. Figure 1b shows portion of the finite element mesh, with an average element quality of 0.82. To determine the optimal mesh size, a sensitivity analysis was performed in the model. These findings suggested that the selected mesh size is appropriate to accurately simulate the behavior of the system under investigation. The element quality was measured using a built-in assessment based on equiangular skew, which provides a rating between 0 and 1 [7,10]. It should be noted that all the domains in the model had a quality of more than 0.5.

Mechanical properties

Mechanical properties define how materials respond to applied forces or loads [26]. Table 1 provides information about the mechanical properties of the porcine eye that have been successfully used in previous models [5,24]. Young's modulus measures how stiff a material is, specifically its resistance to stretching or compression, while Poisson's ratio describes how a material deforms laterally (sideways) when it is stretched or compressed along its length. Although some materials may behave in a non-linear way, Krag and Andreassen have discussed that assuming linearity is a reasonable approximation as long as the strain remains below 10% [14]. Therefore, for the purposes of this model, we make the assumption that each material is linearly elastic and isotropic.

Table 1. Material properties of the porcine eye (the typical values are highlighted in grey).

Modelled parts		Density [kg/m3]	Young's modulus [MPa]	Poisson's ratio [-]
Sclera	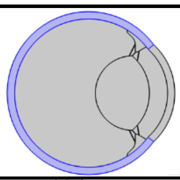	1400	0.1 E_s=2.8	υ_s=0.45
			0.5 E_s=1.4	υ_s=0.46
			E_s=28.0	υ_s=0.47
			2 E_s=56.0	υ_s=0.48
			10 E_s=280.0	υ_s=0.49
Cornea	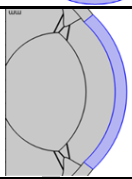	1400	0.1 E_c=1.2	υ_c=0.45
			0.5 E_c=6.0	υ_c=0.46
			E_c =12.0	υ_c=0.47
			2 E_c=24.0	υ_c=0.48
			10 E_c=120.0	υ_c=0.49
Muscle	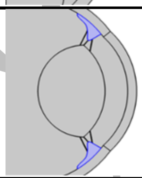	1600	0.1 E_m=1.1	υ_m=0.45
			0.5 E_m=5.5	υ_m=0.46
			E_m =11.0	υ_m=0.47
			2 E_m=22.0	υ_m=0.48
			10 E_m=110.0	υ_m=0.49
Lens	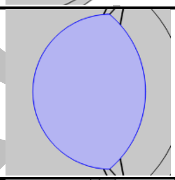	1100	0.1 E_l=0.15	υ_l=0.45
			0.5 E_l=0.75	υ_l=0.46
			E_l =1.50	υ_l=0.47
			2 E_l=3.00	υ_l=0.48
			10 E_l=15.00	υ_l=0.49
Zonule fibres	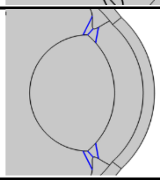	1000	0.1 E_z=0.095	υ_z=0.45
			0.5 E_z=0.475	υ_z=0.46
			E_z =0.950	υ_z=0.47
			2 E_z=1.900	υ_z=0.48
			10 E_z=9.500	υ_z=0.49

To have the impact of intraocular pressure (IOP) on the ocular structure, an IOP of 15 mmHg was applied to the inner surfaces of the sclera, lens, and ciliary body [19], by modeling the vitreous body and aqueous humour as a viscous Newtonian incompressible fluid with this initial pressure. For this media, dynamic viscosity and density are of 0.00074 Pa·s and 1000 kg/m^3 respectively [27].

Sensitivity analysis

Sensitivity analysis in FEM involves studying how changes in input parameters affect the outcomes of the mechanical model. By varying parameters such as geometry, material properties, boundary conditions, mesh size, and loads, the impact can be assessed on the results. This analysis helps to understand the sensitivity to different inputs and then identify critical parameters that significantly influence the behavior of the model [6,21]. Figure 3 illustrates the sequential steps involved in conducting sensitivity analysis.

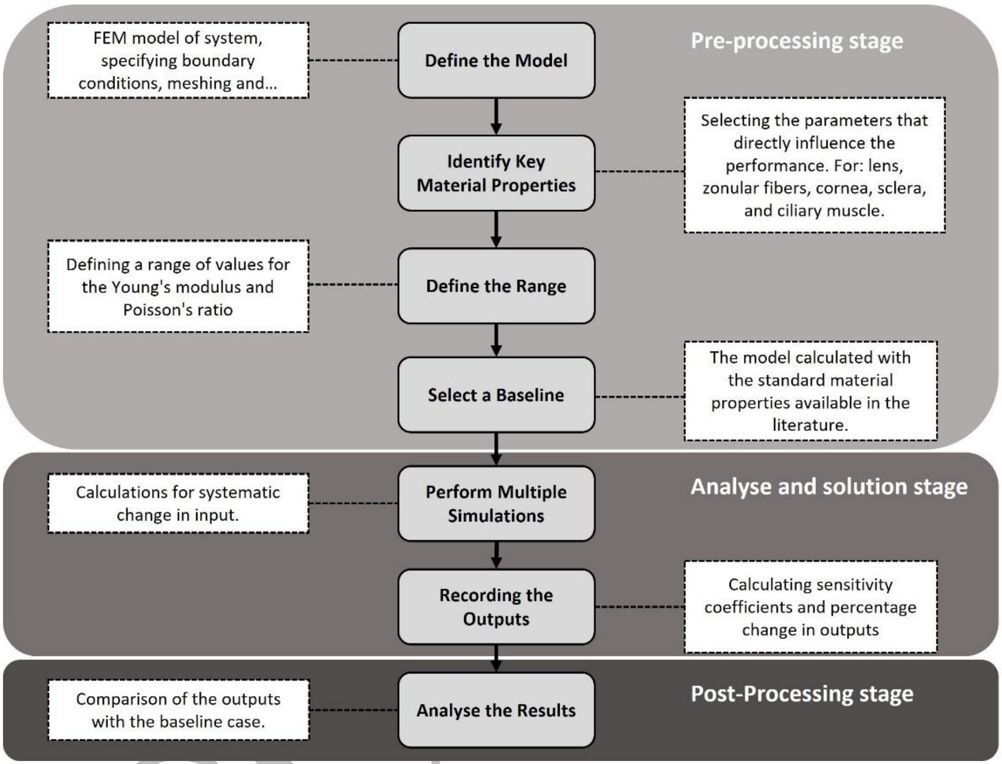

Figure 3. Graphical representation of the steps taken to perform the sensitivity analysis.

In the current study, in particular, we focused on material properties, including different values of Young's modulus and Poisson's ratio for ocular tissues to conduct the sensitivity analysis. The effect of these values on the mechanical displacement amplitude of crystalline lens apex (crystalline lens overshooting), with the different coefficients in Table 1, will be investigated. These coefficients are divided into two groups: first, the Young's modulus ranges from [0.1, 0.5, 1, 2, and 10] times the value of Young's modulus [5] that was most frequently referred in previous models, while second, the Poisson's ratio ranges between [0.45, 0.46, 0.47, 0.48, and 0.49] comparable to the Vannah et al. study [29]. In total, 40 simulations were performed for the parameters of interest.

In addition, to quantify the displacement of the crystalline lens apex as an inertial effect, the time of maximum displacement appearance, and the maximum displacement and stabilization time will be considered (see Figure 4 for explanation). The time of maximum displacement signifies when the maximum lens displacement occurs (t_{peak}), stabilization time denotes the time point when the lens returns or recover to 10% of its total displacement ($t_{balance}$), and maximum displacement D_{max} quantifies the apex position of the crystalline lens displacement at the t_{peak}.

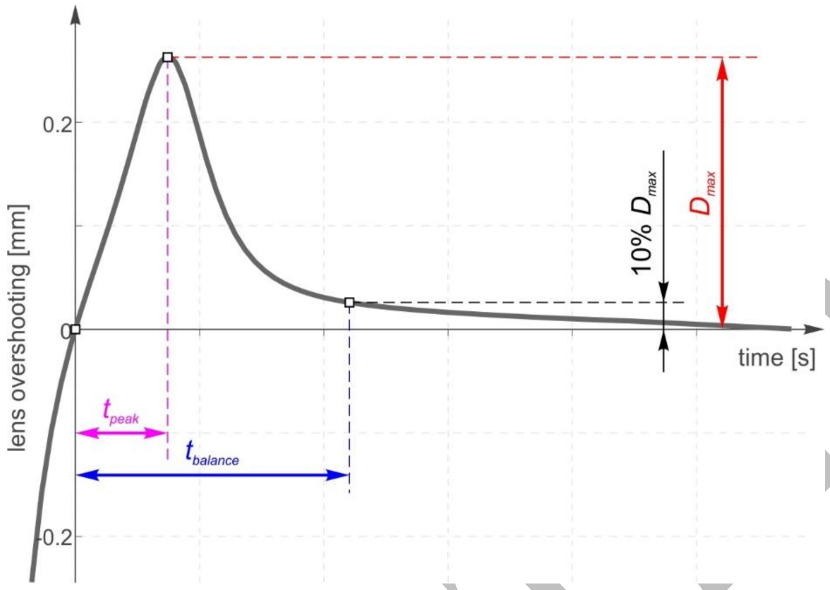

Figure 4. Quantified parameters of the crystalline lens apex displacement.

3. Results

3.1. Young's Modulus

Examining the biomechanical responses of the eye components at different E values has revealed characteristic outputs. To measure the outcome parameter, we determined the difference (percentage difference in Figure 6, 7, and 8) in the parameters of interest compared to a previously validated standard model. Quantitative data was analyzed to compare the three outcome factors, as described in Table 2. Further, the displacement magnitude graphs (Figure 5) clearly highlight the variations.

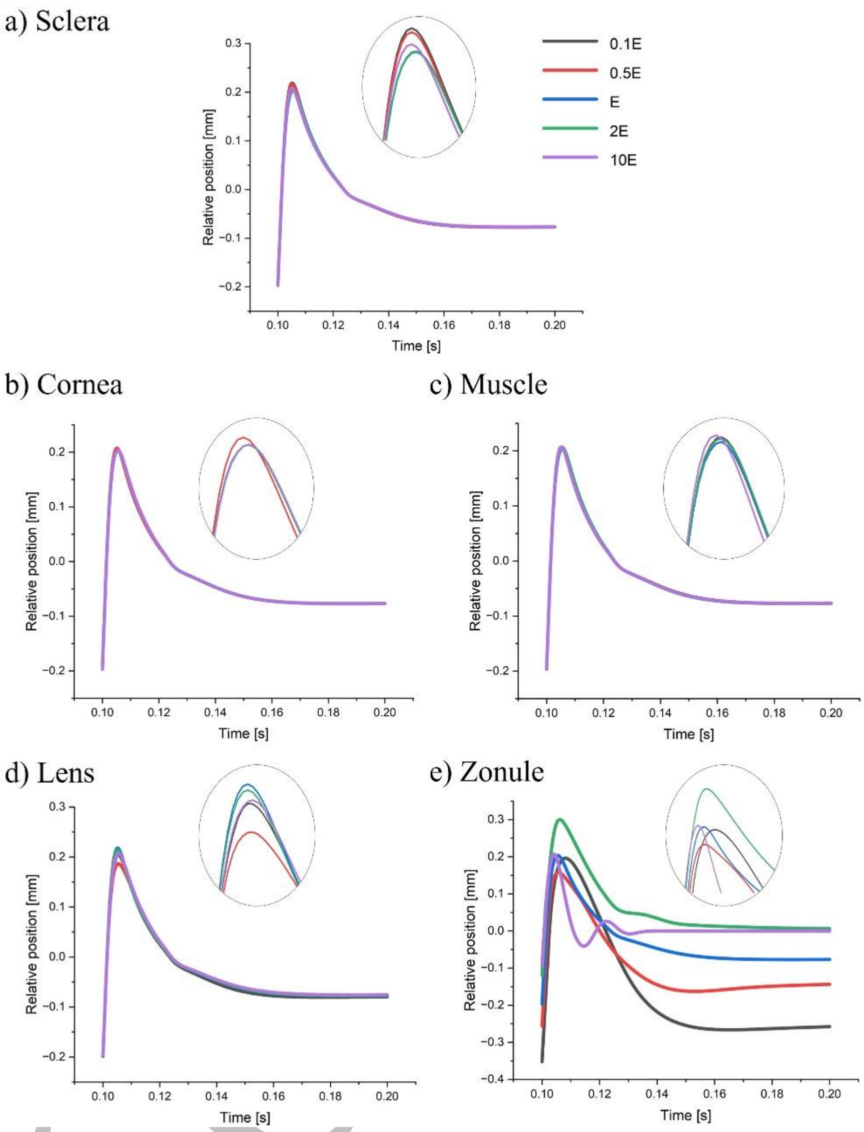

Figure 5. Displacement magnitude in the lens under varying conditions of Young's modulus in different parts of the eye.

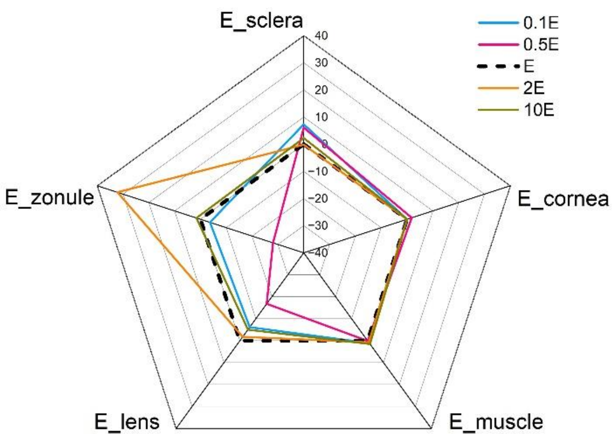

Figure 6. Percentage share of variations in D_{max} for different Young's modulus used in the model components.

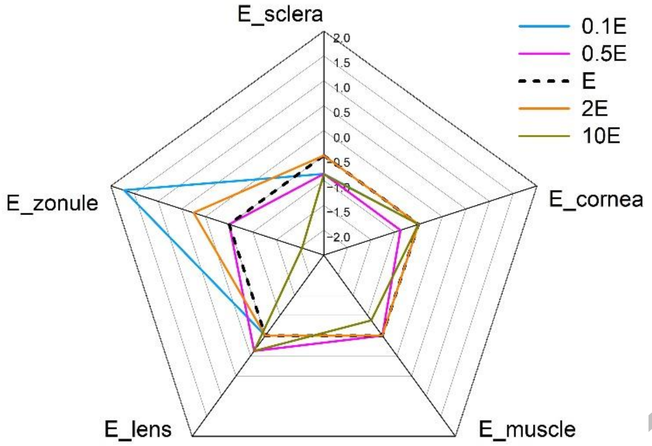

Figure 7. Percentage share of variations in t_{peak} for different Young's modulus used in the model components.

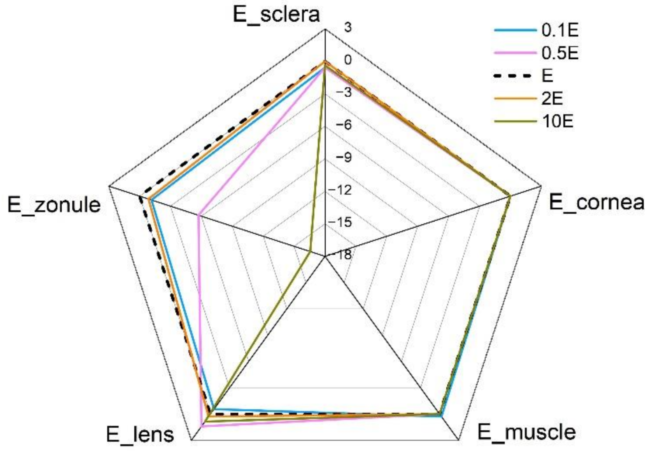

Figure 8. Percentage share of variations in $t_{balance}$ for different Young's modulus used in the model components.

Table 2. Different Young's modulus values and corresponding: maximum displacement (D_{max}), time of maximum displacement (t_{peak}), and stabilization time ($t_{balance}$) for various tissues (sclera, cornea, muscle, lens, and zonule). Each row involves the alteration of the Young modulus of the specific tissue, while the typical value for the other tissues remains unaltered.

Parameter value	0.1 *E*			0.5 *E*			*E*			2 *E*			10 *E*		
	D_{max}*	t_{peak}**	$t_{balance}$***	D_{max}	t_{peak}	$t_{balance}$	D_{max}	t_{peak}	$t_{balance}$	D_{max}	t_{peak}	$t_{balance}$	D_{max}	t_{peak}	$t_{balance}$
Sclera	0.219	0.105	0.140	0.216	0.105	0.140	0.204	0.106	0.141	0.203	0.106	0.141	0.208	0.105	0.141
Cornea	0.204	0.106	0.141	0.208	0.105	0.141	0.204	0.106	0.141	0.204	0.106	0.141	0.204	0.106	0.141
Muscle	0.206	0.106	0.141	0.204	0.106	0.141	0.204	0.106	0.141	0.206	0.106	0.141	0.207	0.105	0.141
Lens	0.205	0.105	0.139	0.187	0.106	0.142	0.204	0.106	0.141	0.214	0.105	0.140	0.207	0.106	0.141
Zonule	0.196	0.108	0.139	0.159	0.106	0.133	0.204	0.106	0.141	0.300	0.106	0.140	0.207	0.104	0.121

* maximum displacement [mm] ** time of maximum displacement [s] *** stabilization time [s]

Sclera

Sclera plays a crucial role in maintaining the external shape of the eye and providing structural support, and it consistently exhibits a particular trend. As the parameter value increases, there is a systematic reduction in D_{max}, indicating a potential inverse relationship with the stiffness or rigidity of the sclera. Remarkably, the time-related parameters, t_{peak} and $t_{balance}$, remain stable across different conditions, implying a reliable and reproducible response pattern. This stability in temporal characteristics suggests that sclera serves as a structural foundation, highlighting the importance of maintaining equilibrium during dynamic eye movements.

As shown in Figure 5a, even slight changes in Young's modulus resulted in noticeable differences in the displacement magnitude, highlighting the crucial role of the material's stiffness in influencing the mechanical behavior of the eye lens.

The investigation of D_{max} percentages under different values of the sclera Young's modulus (E_s) shows different findings compared to the standard model (Figure 6). In particular, a consistent reduction of approximately 0.38% observed under $0.1{\cdot}E_s$ and $0.5{\cdot}E_s$, relative to the standard model. However, no noticeable change in the t_{peak} was observed under $10{\cdot}E_s$ (Figure 7). The presence of negative values in the $t_{balance}$ under $0.1{\cdot}E_s$ and $0.5{\cdot}E_s$ indicated a delayed balance compared to the standard model (Figure 8). In contrast, positive values were observed under $0.1{\cdot}E_s$ and $0.5{\cdot}E_s$, indicating an increase in displacement. $2{\cdot}E_s$ exhibited a slight negative displacement, while $10{\cdot}E_s$ demonstrated a clear escalation in displacement compared to the standard model.

Cornea

As can be seen in Table 2 by changing cornea Young's modulus (E_c), the cornea maintains an approximate stability in D_{max}. This is not surprising, given the cornea's vital role in refracting light and its sensitivity to external forces. Despite variations in mechanical stimuli, time-related parameters remain constant, indicating that the Cornea maintains a consistent temporal response (Figure 5b). These observations are significant in understanding the resilience of the cornea and its ability to maintain visual acuity under different biomechanical conditions.

The evaluation of D_{max} with respect to various E_c, demonstrated dynamic responses that differed from the standard model. In particular, there was a small decrease of approximately 0.38% under $0.5{\cdot}E_c$, while consistency with the standard model was maintained across all elasticity constants (Figure 7). also $0.5{\cdot}E_c$ showed a decrease in t_{peak} (Figure 7), where as other elasticity constants presented only slight variations compared to the standard model. From Figure 8, there was no evidence that E_c had an influence on $t_{balance}$.

Ciliary muscle

The muscle component, responsible for eye movement and positioning, exhibits small variations in D_{max} (Table 2). These findings contribute to our understanding of how ocular muscles adapt under different biomechanical conditions. Similarly, as Figure 7 and 8 show, the time-related parameters did not show any significant changes compared to the standard model, indicating that the temporal aspects of the muscle response are robust and resistant to changes in mechanical input.

Crystalline Lens

Crystalline lens, an essential component for directing light onto the retina, displays more changes, as observed in Table 2. It is worth noting that D_{max} shows a decline when the Young's modulus of the lens (E_l) is reduced by half. and a rise at $2{\cdot}E_l$, indicating a possible sensitivity to intermediate parameter values. Minor fluctuations in D_{max} were identified for remaining values. Analysis of lens displacement percentages across different elasticity constants (E_l) revealed different patterns compared to the standard model (Figure 6).

The time-related parameters, particularly the t_{peak}, demonstrate sensitivity to changes in E_l (Figure 7), implying that the movement of the lens is influenced by the mechanical surroundings. These observations emphasize the complex relationship between parameter values and the optical attributes of the lens, providing valuable insight into factors that could affect visual clarity. An elasticity constant of $0.5{\cdot}E_l$ and $10{\cdot}E_l$ displayed a positive value, indicating an extended time for a peak displacement. However, other elasticity constants did not show significant deviations from the baseline.

In the same way, minor variations in $t_{balance}$ were observed for other elasticity constants compared to the baseline. The $0.1{\cdot}E_l$, indicating a decrease. On the other hand, an elasticity constant of $2{\cdot}E_l$, $10{\cdot}E_l$ and $0.5{\cdot}E_l$ displayed a slight positive shift relative to the baseline (Figure 8).

Zonular fibers

The zonules, which play a crucial role in supporting the lens and enabling accommodation, demonstrate remarkable responsiveness. Table *2* provides an overview of the findings. D_{max} experiences notable changes (Figure 6), particularly with a maximum achieved at $2{\cdot}E_z$ (zonular fibers Young's modulus), suggesting a increased vulnerability to modifications in parameter values. Other D_{max} are significantly affected by E_z.

The time-related parameters display variability, provided in Figure 7 and 8, which highlights the delicate equilibrium necessary for effective lens stabilization. A drop in $t_{balance}$ and t_{peak} is observed with $10{\cdot}E_z$. These findings suggest that lower elasticity ($0.1{\cdot}E_z$) tends to just expand time-related parameters without placing an important impact on D_{max}. In a different pattern, $0.5{\cdot}E_z$ indicates reductions in D_{max} and t_{balance} with no significant shifting in t_{peak}. These discoveries underscore the importance of understanding the mechanical response of the Zonula within the realm of ocular biomechanics and its potential impact on conditions that affect lens accommodation.

A concise summary is presented here to show the different displacement patterns in the lens and how they are directly related to varying E_z values, as seen in Figure 5. Zonular fibers are identified as the most important part, followed by the lens, sclera, ciliary body, and cornea. The changes that took place in all displacement phases will be explained below:

- *early phase* 0.01 - 0.02 s: the lens experiences a settling phase at different E_z values, characterized by negative displacement, before transitioning to positive displacement.
- *mid phase* 0.02 - 0.08 s: positive displacement tends to intensify, and oscillations become more pronounced at higher E_z values. It should be noted that the values of $0.5{\cdot}E_z$ and E_z display distinct peaks during this phase.
- *late phase* 0.08 s onwards: the lens appears to attain a relatively stable state as the displacement stabilizes, with the highest positive displacement being observed at $10{\cdot}E_z$, while the oscillations gradually decrease.

3.2. Poisson's Ratio

Another aim of this study was to assess how different Poisson's ratios affect the parameters. The influence of lens displacement (Figure 9) is clearly attributed solely to the zonules, as none of the other components provides a notable effect.

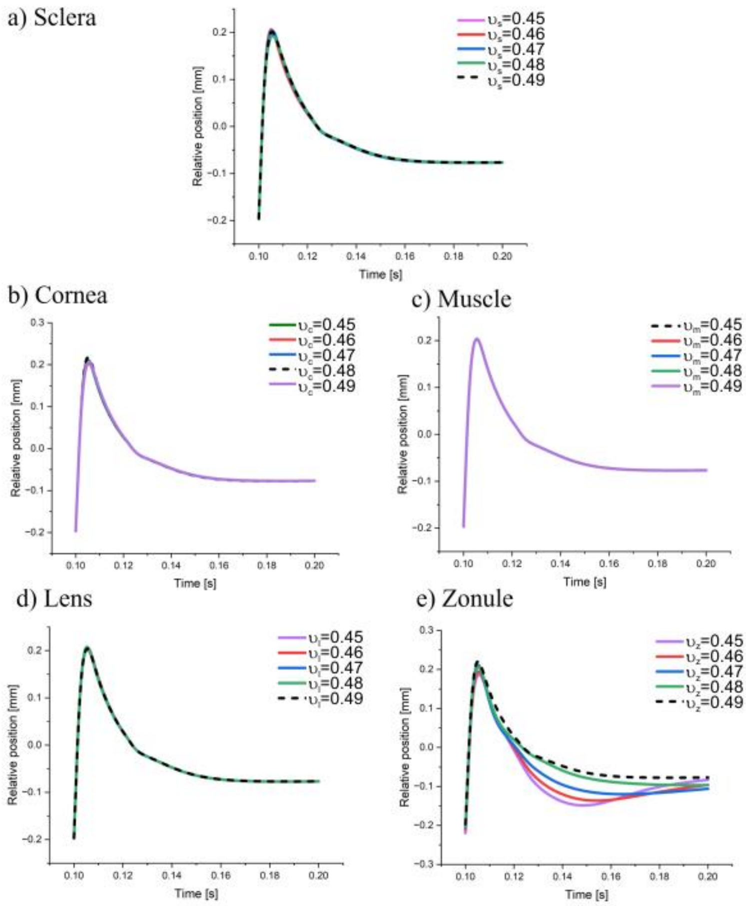

Figure 9. Displacement magnitude in the lens under varying conditions of Poisson's Ratio in different structures of the eye.

Certainly, zonule's Poisson's ratio υ_z plays an essential role for modifying lens displacement, and Table 3 provides numerous important factors to support this theory.

- ***D_{max}*:** the examination demonstrates a marked dependence on the Poisson's ratio. With a decrease in the Poisson's ratio υ_z from 0.49 to 0.45, there is a corresponding fluctuated reduction in D_{max}, indicating that the deformation of the zonule becomes more prominent with lower Poisson's ratios. The values range from 0.187 to 0.221 mm.
- ***t_{peak}*:** minimal variation is observed in the t_{peak}, across various Poisson's ratios. The temporal dimension seems to show a relatively consistent.
- ***$t_{balance}$*:** the duration necessary for equilibrium is affected by the Poisson's ratios. Lower Poisson's ratios are associated with longer $t_{balance}$ values.

Table 3. Different Poisson's ratio values for the zonular fibers and its corresponding effect on maximum displacement (D_{max}), time of maximum displacement (t_{peak}), and stabilization time ($t_{balance}$).

Parameter	υ_z=0.45	υ_z=0.46	υ_z=0.47	υ_z=0.48	υ_z=0.49
D_{max} [mm]	0.187	0.195	0.212	0.206	0.221
t_{peak} [s]	0.106	0.106	0.105	0.106	0.105
$t_{balance}$ [s]	0.124	0.127	0.133	0.143	0.140

Taken together, as shown in Figure 10, the analysis of υ_z declares that the t_{peak} remains approximately unaffected, while the $t_{balance}$ presents a steady decline. Furthermore, D_{max} demonstrates more pronounced increase compared to the baseline.

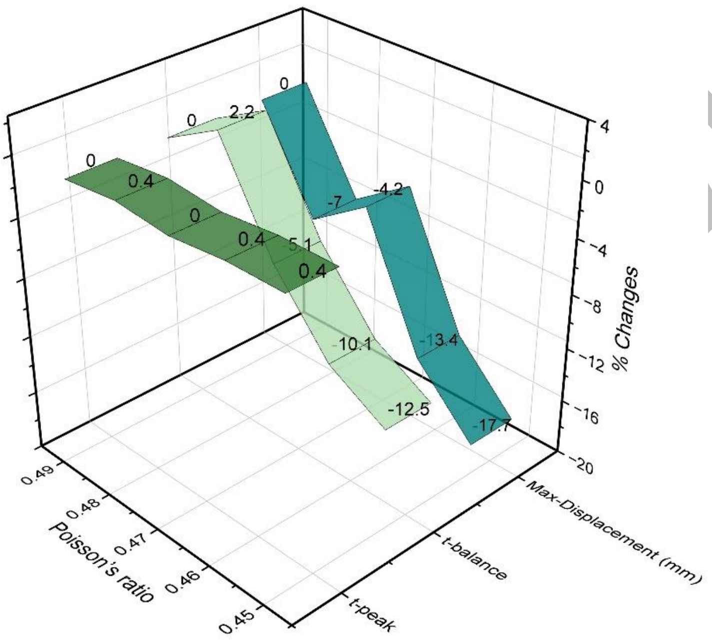

Figure 10. Percentage share of variations in t_{peak}, $t_{balance}$ and D_{max} for different Poisson's ratio values used for zonular fiber.

4. Discussion

Live tissues are known to possess a higher degree of elasticity and flexibility compared to deceased tissues. This inherent characteristic enables living tissues to undergo deformation and subsequently recover their original shape. In contrast, once an organism ceases to live, the tissues gradually lose their elasticity, leading to an increase in stiffness and damping factor. An illustrative example of this phenomenon is rigor mortis, which refers to the stiffening of muscles after death [13]. In *ex vivo* tests, tissue death triggers relaxation of the ciliary body, which prompts the contraction of the zonules, leading to a thinner lens. This state is similar to the non-accommodative or relaxed state of the eye, which is often associated with the initial peak of wobbling, known as overshooting. It is important to note that *ex vivo* tissues do not show wobbling, as confirmed by previous research on eye accommodation [20]. In current research, our objective was to investigate the impact of adjusting the parameters (Mechanical Parameters) of interest on the outcome results.

Through a detailed examination of the biomechanical responses of essential eye components under varying parameter values, researchers can gain valuable insights into the complex dynamics that govern ocular behavior. The findings presented in Figure 5 serve as a catalyst for a detailed discussion on several key aspects, including the significance of E_z in lens mechanical displacement and the broader implications for ocular health. Other findings suggest that a critical value can be associated with zonule's Young's modulus, that would enable it to differentiate between living and non-living tissues. It has been observed that in case of non-living tissues a lack of any oscillation or any periodic characteristic in crystalline lens' interial motion can be observed. Therefore, we have demonstrated that when Young's modulus falls below the threshold of approximately 2 MPa, the tissue behaves similarly to non-living tissue (Figure 5e). This leads to a loss of elasticity and an increased significance of the damping factor. Additionally, the Poisson's ratio of the zonules is a crucial parameter that should be given some more consideration. When the Poisson's ratio is less than 0.48, a minimum peak starts to appear, which we avoid in *ex vivo* patterns. Hence, a Poisson's ratio greater than 0.48. Given our preference for mechanical displacement graphs that closely resemble experimental graphs, it is important to note that we are actively striving to eliminate the wobbling effect. This is due to the fact that a greater similarity to experimental graphs is desired.

As evidenced by the observed changes in lens displacement, lower values of E_z resulted in gradual and smooth displacement, while higher values of E_z led to faster and pronounced responses. The temporal dynamics of this phenomenon revealed distinct phases, including early-phase, mid-phase oscillations, and a late-phase steady state, all of which contributed to the overall mechanical profile. The observation of mid-phase oscillations in lens displacement provides significant information regarding the dynamic nature of the lens lesponse. These oscillations can potentially be influenced by factors such as the E_z and υ_z.

The significant increase in D_{max} at $2 \cdot E_z$ draws attention to the increased vulnerability of this component to specific parameter values, this is because tissue's stability improves as the elasticity (E) of the Zonulas increases. Nevertheless, there exists a threshold beyond which the tissue's desired peak cannot be achieved due to the presence of excessively rigid Zonulas. This finding has the potential to influence lens accommodation and calls for a more accurate *in-silico* model to better mimic lens displacement. This observation emphasizes the importance of considering the mechanical behavior of the zonules in relation to the conditions that affect lens function and accommodation.

Investigations on the influence of the Poisson's ratio on zonular behavior lead to notable outcomes. The observed variations in D_{max}, t_{peak} and $t_{balance}$ shed light on the complex relationship between zonular properties and eye movement. The correlation between decreasing Poisson's ratios and D_{max} implies that zonular deformation becomes more prominent when the elastic responsiveness is reduced. This discovery has significant implications for comprehending the mechanical characteristics of zonules and their contribution to the overall movement of the eye. The increased D_{max} may be linked to changes in the tension and elasticity of zonular fibers, which can affect the transmission of forces within the eye.

An unexpected observation was that the temporal consistency of the t_{peak} remains relatively constant across various Poisson's ratios. This observation suggests that the moment of maximum zonular deformation likely seems to occur uniformly, irrespective of the material properties of the zonules. Such findings may suggest the existence of a finely regulated and coordinated mechanism that governs the timing of zonular responses during eye movements, highlighting the intricate nature of ocular biomechanics. In contrast to t_{peak}, the achievement of balance, known as $t_{balance}$ shows an evident change. This implies that the zonules need shorter time to restore equilibrium after deformation. This fact in time may have implications for the effectiveness of ocular movements, especially in scenarios that demand swift adjustments. This observation highlights the importance of considering future refinements to the model, including the viscoelastic behavior of the zonules and potential adjustments in their number and attachment regions.

5. Conclusions

This comprehensive study of crystalline lens displacement under varying material properties provides a cohesive outlook on the intricate biomechanical responses that govern ocular dynamics. The varying patterns observed in the sclera, cornea, muscle, lens, and, in particular, zonules emphasize the importance of considering tissue biomechanics. The results of the wobbling and overshooting data demonstrate that fine-tuning these parameters exclusively can yield a remarkable model, facilitating extensive investigations in this particular field. They show that the pivotal factors in modeling the *ex vivo* porcine eye overshooting are zonule's Young's modulus and Poisson's ratio. This finding enable us to focus specifically on the effects of IOP in future study.

Recognizing the limitations of this study, such as the *ex vivo* nature and the 2D simplified model utilized, influences of varying IOP, the absence of turnovering outflow dynamics at the trabecular meshwork, and the role of nonlinear material, is essential. To enhance the depth and applicability of our understanding, future investigations should consider incorporating *in vivo* data and other biomechanical factors, including the effect of increased IOP [8,9] on the geometry of the eye and – potentially – on the wobbling outucomes. This eventual effect will be addressed in our next study.

Overall, the study discussed in this research paper offers new avenues for future research in the field of ophthalmology, particularly in relation to understanding and addressing conditions that are influenced by the dynamic aspects of the eye, such as estimating IOP and predicting glaucoma.

Data availability statement

The original contributions presented in the study are included in the article/Supplementary Material; further inquiries can be directed to the corresponding author.

Declaration of competing interest

The authors declare that they have no known competing financial interests or personal relationships that could have appeared to influence the work reported in this paper.

Funding

The author(s) declare financial support was received for the research, authorship, and/or publication of this article. AD is an ESR in the OBERON project funded within the framework of the European Union’s Horizon 2020 Research and Innovation Program under the Marie Skłodowska-Curie grant agreement No. 956720. MS, AB, and DS: grant number 2019/35/B/ST7/03998 (National Science Center, Poland). FEM simulations were carried out using resources provided by Wroclaw Center for Networking and Supercomputing (http://wcss.pl), grant number 556.

Supplementary material

S1: Animation presenting the lens inertial overshooting.

S2: Illustration of decentration and tilt of the crystalline lens being induced by rotation motion of the whole eye globe. Lens decentration refers to the misalignment of the optical center of the lens with the center of the lens mount. Lens tilt refers to the angular misalignment of the lens relative to the optical axis of the eye globe.

References

1. Ayyalasomayajula A., Park R.I., Simon B.R., Vande Geest J.P., A porohyperelastic finite element model of the eye: the influence of stiffness and permeability on intraocular pressure and optic nerve head biomechanics, Comput Methods Biomech Biomed Eng, 2016, 19(6):591-602.
2. Bocskai Z. Bojtár I., Biomechanical modelling of the accommodation problem of human eye, Period Polytech Civ Eng, 2013, 57(1):3-9.
3. Boszczyk A., Dębowy F., Jóźwik A., Dahaghin A., Siedlecki D., Complexity of crystalline lens wobbling investigated by means of combined mechanical and optical simulations, Biomed Opt Express, 2023, 14(6):2465-2477.
4. Coldrick B., Modelling the human accommodation system using finite element analysis, Dissertation, Aston University, 2013.

5. Dahaghin A., Salimibani M., Boszczyk A., Jóźwik A., Skrok M., Grasa J., Siedlecki D., Investigation of the crystalline lens overshooting: ex-vivo experiment and opto-mechanical simulation results, Front Bioeng Biotechnol, 2024, 12, DOI: 10.3389/fbioe.2024.1348774 p. 1348774.
6. Dahaghin A., Salimibani M., Boszczyk A., Siedlecki D., Effect of Tissue Parameters on the Dynamics of Crystalline Lens Overshooting, Invest Ophthalmol Vis Sci, 2024, 65(7):5041.
7. Etminan A., Salimibani M., Dahaghin A., Haghpanahi M., Maleki A., FEM thermal assessment of a 3-D irregular tumor with capillaries in magnetic nanoparticle hyperthermia via dissimilar injection points, Comput Biol Med, 2023, 157, DOI: 10.1016/j.compbiomed.2023.106771.
8. Genest R., Chandrashekar N., Irving E., The effect of intraocular pressure on chick eye geometry and its application to myopia, Acta Bioeng Biomech, 2012, 14(2):3-8.
9. Hoffmann E.M., Aghayeva F., Wagner F.M., Fiess A., Nagler M., Münzel T., Wild P.S., Beutel M.E., Schmidtmann I., Lackner K.J., Pfeiffer N., Schuster A.K., Intraocular Pressure and Its Relation to Ocular Geometry: Results From the Gutenberg Health Study, Invest Ophthalmol Vis Sci, 2022, 63(1), DOI: 10.1167/iovs.63.1.40.
10. Issarti I., Koppen C., Rozema J.J., Influence of the eye globe design on biomechanical analysis, Comput Biol Med, 2021, 135, DOI: 10.1016/j.compbiomed.2021.104612.
11. Kampmeier J., Radt B., Birngruber R., Brinkmann R., Thermal and biomechanical parameters of porcine cornea, Cornea, 2000, 19(3):355-363.
12. Karimi, A., Rahmati S.M., Razaghi R., Girkin C.A., Crawford Downs J., Finite element modeling of the complex anisotropic mechanical behavior of the human sclera and pia mater, Comput Methods Programs Biomed, 2022, 215, DOI: 10.1016/j.cmpb.2022.106618.
13. Kori S., Time since death from rigor mortis: forensic prospective, J Forensic Sci & Criminal Inves, 2018, 9:1-10.
14. Krag S., Andreassen T.T., Mechanical properties of the human lens capsule, Prog Retin Eye Res, 2003, 22(6):749-767.
15. Lanchares E., Navarro R., Calvo B., Hyperelastic modelling of the crystalline lens: Accommodation and presbyopia, J Optom, 2012, 5(3):110-120.
16. Ljubimova D., Eriksson A., Bauer S., Numerical study of the effect of vitreous support on eye accommodation, Acta Bioeng Biomech, 2005, 7(2):3-16.
17. Martin H., Bahlke U., Guthoff R., Rheinschmitt L., Schmitz K.P., Determination of inertia forces at an intraocular lens implant during saccades. in World Congress on Medical Physics and Biomedical Engineering, September 7-12, 2009, Munich, Germany: Vol. 25/11 Biomedical Engineering for Audiology, Ophthalmology, Emergency & Dental Medicine. Springer, 2009.
18. Menduni F., Davies L.N., Madrid-Costa D., Fratini A., Wolffsohn J.S., Characterisation of the porcine eyeball as an in-vitro model for dry eye, Cont Lens Anterior Eye, 2018, 41(1):13-17.
19. Muñoz Sarmiento D.M., Rodríguez Montaño Ó.L., Alarcón Castiblancoa J.D., Cortés Rodríguez C.J., The impact of horizontal eye movements versus intraocular pressure on optic nerve head biomechanics: A tridimensional finite element analysis study, Heliyon, 2023. 9(2), DOI: 10.1016/j.heliyon.2023.e13634.
20. Nyström M., Andersson R., Magnusson M., Pansell T., Hooge I., The influence of crystalline lens accommodation on post-saccadic oscillations in pupil-based eye trackers, Vision Res, 2015. 107:1-14.
21. Olhoff N., Lund E., Finite element based design sensitivity analysis and optimization in: Jose Herskovits (Ed.) Advances in Structural Optimization, Kluver Academic Publishers, 2005.
22. Redaelli E., Grasa J., Calvo B., Rodriguez Matas J.F., Luraghi G., A detailed methodology to model the Non Contact Tonometry: a Fluid Structure Interaction study, Front Bioeng Biotechnol, 2022, 10, DOI: 10.3389/fbioe.2022.981665.
23. Regal S., Troughton J., Djenizian T., Ramuz M., Biomimetic models of the human eye, and their applications, Nanotechnol, 2021, 32(30), DOI: 10.1088/1361-6528/abf3ee..

24. Rossi T., Boccassini B., Esposito L., Iossa M., Ruggiero A., Tamburrelli C., Bonora N., The pathogenesis of retinal damage in blunt eye trauma: finite element modeling, Invest Ophthalmol Vis Sci, 2011, 52(7):3994-4002.
25. Ruan, C., Yu Q., Zhou J., Ou X., Liu Y., Chen Y., Fluid-structure interaction simulation for studying hemodynamics and rupture risk of patient-specific intracranial aneurysms, Acta Bioeng Biomech, 2023, 25(3):73-85.
26. Rusińska, M., Gruber P., Ziółkowski G., Łabowska M., Wilińska K., Szymczyk-Ziółkowska P., The influence of Material Extrusion process parameters on the porosity and mechanical properties of PLA products for medical applications, Acta Bioeng Biomech, 2023, 25(3):25-41.
27. Singh D., Firouzbakhsh K., Ahmadian M.T., Human intraocular thermal field in action with different boundary conditions considering aqueous humor and vitreous humor fluid flow, Int J Mech Mechatron Eng, 2017, 11(4):717-725.
28. Tabernero J., Artal P., Lens oscillations in the human eye. Implications for post-saccadic suppression of vision, PloS one, 2014. 9(4), DOI: 10.1371/journal.pone.0095764.
29. Vannah W.M., Childress D.S., Modelling the mechanics of narrowly contained soft tissues: the effects of specification of Poisson's ratio, J Rehabil Res Dev, 1993. 30:205-209.
30. Wang K., Venetsanos D.T., Hoshino M., Uesugi K., Yagi N., Pierscionek B.K., A modeling approach for investigating opto-mechanical relationships in the human eye lens, IEEE Trans Biomed Eng, 2019, 67(4):999-1006.
31. Yan Y., Shi H., Zhao Y., Cao Y., Xie Z., Correlation study of biomechanical changes between diabetic eye disease and glaucoma using finite element model of human eye with different iris-lens channel distances, Med Eng Phys, 2022, 109, DOI: 10.1016/j.medengphy.2022.103910.
32. Zhou B., Sit A.J., Zhang X., Noninvasive measurement of wave speed of porcine cornea in ex vivo porcine eyes for various intraocular pressures, Ultrason, 2017, 81:86-92.